$Pa\bar{3}$ Modified Fluorite-Type Structures in Metal Dioxides at High Pressure

J. Haines,* J. M. Léger, O. Schulte

Rutile-structured SnO_2, PbO_2, and RuO_2 have long been known to transform to cubic high-pressure phases, for which a fluorite structure has been assumed. Rietveld refinement results from x-ray diffraction studies indicated that these phases have a modified fluorite structure (space group $Pa\bar{3}$). Thus, for metal dioxides, all known cubic, postrutile phases have the $Pa\bar{3}$ structure, thereby providing experimental examples of the high-pressure structure predicted from theoretical calculations for stishovite (rutile-structured silica). High-pressure transitions in stishovite may have profound implications for the geochemistry of the core–mantle boundary.

The sequence of pressure-induced phase transitions in rutile-structured metal dioxides has been the subject of considerable interest, particularly because these metal dioxides serve as models for the behavior of stishovite at higher pressures. Because of the larger size of the metal cations, the same phase transitions to denser phases as for silica are expected to be observed at lower pressures in metal dioxides.

It has been proposed that rutile-structured SnO_2, PbO_2, and RuO_2 transform to the cubic, fluorite structure at high pressure, with an increase in cation coordination number from 6 to 8 (*1–3*). Previous diffraction experiments indicated that SnO_2 and PbO_2 undergo transitions first to an α-PbO_2–type phase (*4, 5*) and then subsequently to a cubic phase assumed to be fluorite structured (*2, 6, 7*). The volume changes (ΔV) are 2 to 3% for the transition from rutile to α-PbO_2 and 5% for the transition from α-PbO_2 to the cubic phase. In RuO_2, a second-order transition to a $CaCl_2$-type phase was observed before the transformation ($\Delta V = 6.1\%$) to the cubic phase (*3*). The orthorhombic $CaCl_2$ structure (*Pnnm*) is a simple distortion of the tetragonal rutile structure ($P4_2/mnm$), which involves a slight rotation of the columns of edge-sharing octahedra aligned parallel to *z*.

Theoretical calculations indicate, however, that for both SiO_2 and GeO_2 the cubic, postrutile phase should have the $Pa\bar{3}$ modified fluorite structure (*8, 9*). Both theory and experiment show that stishovite undergoes a first transition to a $CaCl_2$-type structure (*8, 10*). Calculations indicate that at pressures of 60 or 150 GPa, respectively, stishovite or $CaCl_2$-type SiO_2 should transform to a modified fluorite structure (space group $Pa\bar{3}$) (*8, 11*). In this modified structure the oxygen atoms are significantly displaced from their positions in the fluorite structure (space group $Fm\bar{3}m$): The oxygen atoms lie on Wyckoff sites 8c (u,u,u) with a positional coordinate of $u = 0.344$ instead of $u = 0.250$ (Fig. 1). In both structures, the Si atoms lie on sites 4*a* (0,0,0) and form a face-centered-cubic sublattice. This displacement of the oxygen atoms distorts the coordination polyhedron from a cube to a regular rhombohedron, yielding a Si coordination number of 6+2 instead of 8. Calculations for GeO_2 have indicated that the $Pa\bar{3}$ phase should become stable relative to the rutile-type phase above 60 GPa (*9*). The only experimentally confirmed example of this $Pa\bar{3}$ structure to date has been that of the high-pressure phase of the fluoride PdF_2 (*12, 13*). No structure refinement has been reported for cubic high-pressure phases of dioxides. The results described here indicate that these metal dioxides adopt the $Pa\bar{3}$ structure instead of the fluorite structure.

Powdered SnO_2, PbO_2, and RuO_2 (Alfa Products), along with ruby powder, and for SnO_2, trace TiC to absorb laser radiation, were placed in holes of 150 to 200 μm in diameter in stainless steel gaskets preindented to a thickness of 120 μm between the anvils of a diamond anvil cell. Silicone grease was used as a pressure-transmitting medium to avoid discontinuities produced above 10 GPa by the freezing of the commonly used 4:1 mixture of methanol and ethanol. Pressures were measured on the basis of the shift of the ruby R_1 fluorescence line (*14*). SnO_2 and RuO_2 were heated to temperatures of about 1000°C with a 50-W Nd-yttrium-aluminum-garnet laser. This increased the rate of transformation and greatly reduced deviatoric stress. In situ high-pressure, angle-dispersive x-ray diffraction patterns and the ambient RuO_2 diffraction pattern were obtained on an imaging plate placed at distances of between 85 and 158 mm from the sample with zirconium-filtered molybdenum radiation collimated to 130 μm from an 800-W fine-focus tube. Exposure times were 24 to 48 hours. Observed intensities were integrated as a function of diffraction angle 2θ to yield standard one-dimensional diffraction patterns. Rietveld refinements were performed with the Fullprof program (*15*).

SnO_2 transformed to a $CaCl_2$-type phase above 4 GPa. A further transformation to the α-PbO_2–type phase started above 12 GPa but was only 15% complete at 19 GPa. The transition from these lower pressure phases to the cubic phase began above 21 GPa. This transition sequence is in good agreement with the results of previous studies (*2, 5, 6, 16*), except that the $CaCl_2$-type phase was not distinguished from the rutile-type phase in the previous studies because of the limited resolution then available. To obtain the greatest proportion of the cubic phase above 24 GPa, we heated the sample. The 210 reflection, systematically absent for the $Fm\bar{3}m$ fluorite structure, was present in the diffraction pattern of the cubic phase (Fig. 2). This is the most intense diffraction line arising from the oxygen sublattice in the $Pa\bar{3}$ structure. Rietveld refinement of the high-pressure data with a $Pa\bar{3}$ structural model yielded $u = 0.347(1)$ with the cubic cell constant $a = 4.8700(2)$ Å at 48 GPa (all figures in parentheses refer to standard deviations and correspond to the last digit or digits). The fit for the $Pa\bar{3}$ model is far superior to that for the $Fm\bar{3}m$ model (Fig. 2). At 48 GPa, the tin ion is surrounded by six oxide anions at 1.991(3) Å and two more distant anion neighbors at 2.924(3) Å. The cubic phase retransformed with the release of pressure to a mixture of the α-PbO_2–type phase and the initial rutile-type phase.

RuO_2 underwent transitions to a $CaCl_2$-

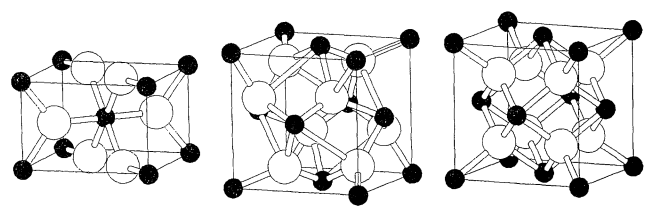

Fig. 1. Tetragonal rutile ($P4_2/mnm$), cubic modified fluorite ($Pa\bar{3}$), and fluorite ($Fm\bar{3}m$) structures. The cations and anions are represented by small filled circles and large open circles, respectively. Note that in the modified fluorite structure there is a short O–O contact at the center of the unit cell, whereas in the fluorite structure there is an empty cubic site. The modified fluorite structure is thus a better candidate for a high-pressure structure.

CNRS, Laboratoire de Physico-Chimie des Matériaux, 1, Place Aristide Briand, 92190 Meudon, France.

*To whom correspondence should be addressed.

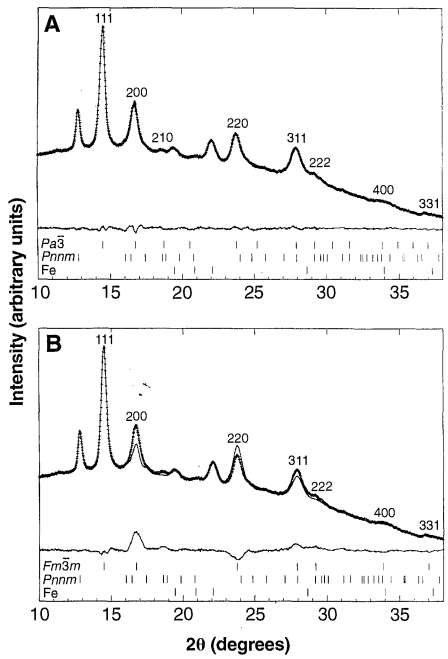

Fig. 2. Experimental (crosses) and calculated (solid line) profiles from Rietveld refinement of SnO_2 at 48 GPa with $Pa\bar{3}$ (**A**) and $Fm\bar{3}m$ (**B**) structural models. Intensity is in arbitrary units; the difference profiles are on the same scale. Vertical bars indicate the calculated positions of diffraction lines of the cubic phase (84% w/w), the remaining $CaCl_2$-type phase (*Pnnm*, 16% w/w), and iron from the gasket (ε-Fe). The diffraction lines of the cubic phase (intensity >3% of the 111 reflection) are indexed. Agreement factors are as follows: R_{Bragg} = 2.3%, R_p = 7.5%, and R_{wp} = 6.1% for the $Pa\bar{3}$ model, and R_{Bragg} = 17.3%, R_p = 19.1%, and R_{wp} = 20.7% for the $Fm\bar{3}m$ model (where p = profile and wp = weighted profile).

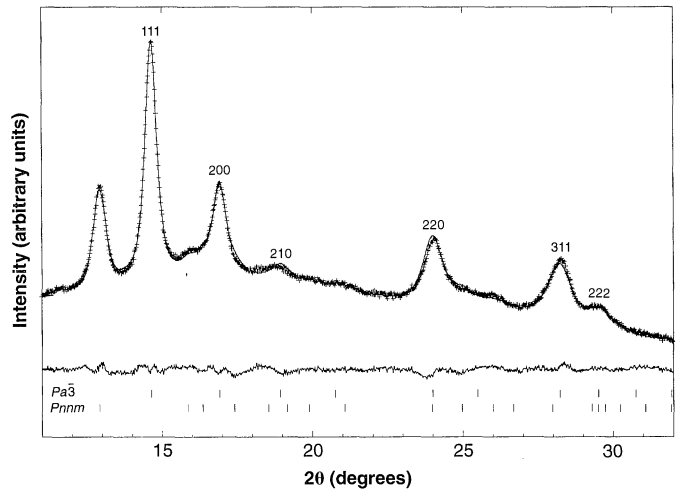

Fig. 3. Experimental (crosses) and calculated (solid line) profiles from Rietveld refinement of RuO_2 at 8.9 GPa. Vertical bars indicate the calculated positions of diffraction lines of the $Pa\bar{3}$ phase (77% w/w) and the remaining $CaCl_2$-type phase (*Pnnm*, 23% w/w). Agreement factors are as follows: R_{Bragg} = 2.2%, R_p = 8.0%, and R_{wp} = 7.1%.

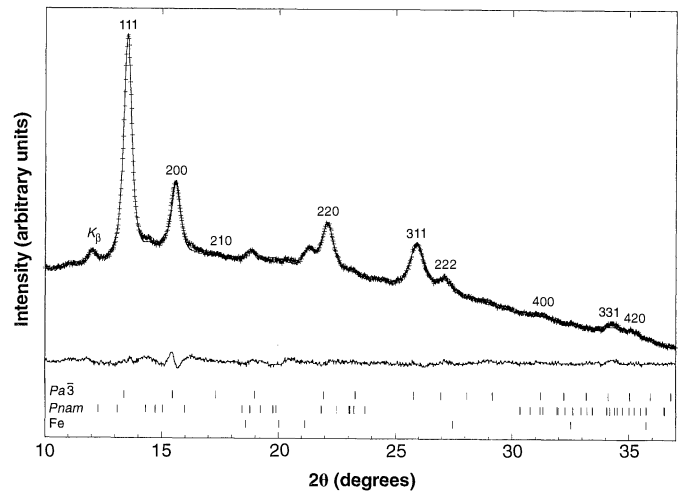

Fig. 4. Experimental (crosses) and calculated (solid line) profiles from Rietveld refinement of PbO_2 at 9.0 GPa. Vertical bars indicate the calculated positions of diffraction lines of the $Pa\bar{3}$ phase (96% w/w), the remaining cotunnite-type phase (*Pnam*, 4% w/w), and iron from the gasket (ε-Fe). Agreement factors are as follows: R_{Bragg} = 4.0%, R_p = 11.0%, and R_{wp} = 8.3%. K_β indicates the most intense reflection due to molybdenum K_β radiation.

type phase below 6 GPa and then to the cubic phase above 12 GPa (*3*). For the greatest conversion to the cubic phase, RuO_2 was compressed to 48 GPa and subsequently heated. The 210 reflection was observed as for SnO_2, indicating that RuO_2 also adopts the $Pa\bar{3}$ structure. Refinement results from the data obtained at 8.9 GPa on decompression (Fig. 3) were u = 0.347(1) and a = 4.8320(3) Å. The $Pa\bar{3}$ phase could be retained down to ambient conditions. Refinement with data obtained on the recovered sample yielded u = 0.347(1) and a = 4.8573(5) Å. The six short and two long polyhedral Ru–O distances were 1.986(5) and 2.918(5) Å, respectively. This compares with eight distances of 2.103 Å for a hypothetical fluorite-type structure with the same volume, whereas rutile-type RuO_2 has four octahedral Ru–O distances of 1.984 Å and two of 1.941 Å (*17*). The minimum O–O distance was 2.578(7) Å in the $Pa\bar{3}$ structure compared with 2.429 Å in a hypothetical fluorite-type structure and 2.468 Å in a rutile-type structure. The O–O distance of 2.578(7) Å in the $Pa\bar{3}$ structure is the distance between rhombohedra along a diagonal of the body of the unit cell. The corresponding distance in a hypothetical fluorite-type structure is 4.207 Å, which is the diagonal of an empty cubic site at the center of the unit cell. The $Pa\bar{3}$ structure is a better candidate for a high-pressure structure because the minimum O–O distance is greater and there is no empty site at the center of the cell (Fig. 1).

PbO_2 transformed from the rutile-type phase to a $CaCl_2$-type intermediate at close to 4 GPa and then to the cubic phase above 7 GPa. The 210 reflection of the $Pa\bar{3}$ structure is calculated to have 1% relative intensity and hence was at the detection limit of the experiment. Despite the low x-ray scattering factor of O^{2-} compared with Pb^{4+}, the difference between the oxygen positions in the fluorite and $Pa\bar{3}$ structures has a significant effect on the relative intensities of the diffraction lines. In particular, the relative intensities of the 200 and 220 reflections for the $Pa\bar{3}$ structure are 37 and 32%, respectively, compared with 30 and 39% for the fluorite structure. The refinement of the cubic phase of PbO_2 was performed at 9.0 GPa after decompression from 30 GPa (Fig. 4). A nearly pure sample of the cubic phase that contained only 4% of the higher pressure cotunnite-type phase was obtained (*18*). The refined a and u values were 5.2804(3) Å and 0.332(2), respectively, yielding six short Pb–O distances of 2.156(8) Å and two long distances of 3.033(8) Å. On pressure release, α-PbO_2 was obtained.

The structural data for the $Pa\bar{3}$ phases of SnO_2, RuO_2, and PbO_2 are compared with those of PdF_2 and with the results of theoretical calculations for SiO_2 and GeO_2 in Table 1. There is good agreement among the u values for the different materials. These u values for the modified fluorite structure lie between those of fluorite (u = 0.25) and pyrite (space group $Pa\bar{3}$, u = 0.37 to 0.40). The pyrite (FeS_2) structure, adopted by many metal chalcogenides and pnictides and some metal peroxides (*19*), is characterized by octahedral metal coordination and dimeric anions.

The present results indicate that all the rutile-type metal dioxides known to transform to a cubic high-pressure phase adopt the modified fluorite structure, rather than

Table 1. Structural data and zero-pressure bulk moduli (B_0) for modified fluorite structures. Experimental data for SnO_2, RuO_2, PbO_2, and PdF_2 were obtained at 48, 8.9, 9.0, and 0.001 GPa, respectively. Theoretical values are those calculated for zero pressure.

Compound	a (Å)	u	B_0* (GPa)	Ref.
		Experimental		
SnO_2	4.8700(2)	0.347(1)	261(14)	†
RuO_2	4.8320(3)	0.347(1)	399‡	†
PbO_2	5.2804(3)	0.332(2)	223(9)	†
PdF_2	5.329(1)	0.3431(4)	§	(*12*)
		Theoretical		
SiO_2	4.40	0.3446	393	(*9*)
SiO_2	4.47	0.344	335	(*11*)
SiO_2	4.41	0.3349	363	(*20*)
SiO_2	4.55	0.337	348.5	(*21*)
SiO_2	4.43	0.344	347	(*21, 22*)
SiO_2	4.41	0.347	387	(*23*)
SiO_2	4.462	0.3445	312	(*24*)
GeO_2	4.643	0.3435	357	(*9*)

*B_0 values were obtained with the Birch-Murnaghan or Murnaghan equations of state (*25*) with first-derivative values between 3.5 and 7 for the experimental data and between 1.6 and 4.4 for the theoretical data. †From the present study. ‡From (*3*). §Not measured.

the fluorite structure assumed previously. The transition to the modified structure corresponds to an increase in cation coordination number from 6 to 6+2 instead of from 6 to 8. There are no remaining examples of a pressure-induced rutile-to-fluorite phase transformation. This represents an important modification to the structural systematics of metal dioxides. The fluorite structure adopted by many compounds under ambient conditions and at high temperatures is not a good candidate for a high-pressure structure because of the empty cubic site at the center of the unit cell. The present observation of transitions in SnO_2, RuO_2, and PbO_2 at high pressures to the $Pa\bar{3}$ structure reconciles the experimental behavior of these metal dioxides with the theoretical predictions for SiO_2 and GeO_2, yielding a common cubic high-pressure structure for these compounds.

REFERENCES AND NOTES

1. L. Liu and W. A. Bassett, *Elements, Oxides and Silicates* (Oxford Univ. Press, New York, 1986).
2. L. C. Ming and M. H. Manghnani, in *High-Pressure Research in Geophysics*, S. Akimoto and M. H. Manghnani, Eds. (Center Academic, Tokyo, 1982), pp. 329–347.
3. J. Haines and J. M. Léger, *Phys. Rev. B.* **48**, 13344 (1993).
4. W. B. White, F. Dachille, R. Roy, *J. Am. Ceram. Soc.* **44**, 170 (1961).
5. L. Liu, *Phys. Earth Planet. Inter.* **9**, 338 (1974).
6. ———, *Science* **199**, 422 (1978).
7. Y. Syono and S. Akimoto, *Mater. Res. Bull.* **3**, 153 (1968).
8. R. E. Cohen, in *High-Pressure Research: Application to Earth and Planetary Sciences*, M. H. Manghnani and Y. Syono, Eds. (American Geophysical Union, Washington, DC, 1992), pp. 425–431.
9. L. H. Jolly, B. Silvi, P. d'Arco, *Eur. J. Mineral.* **6**, 7 (1994).
10. Y. Tsuchida and T. Yagi, *Nature* **340**, 217 (1989); K. J. Kingma, R. E. Cohen, R. J. Hemley, H. K. Mao, *ibid.* **374**, 343 (1995).
11. K. T. Park, K. Terakura, Y. Matsui, *ibid.* **336**, 670 (1988).
12. A. Tressaud, J. L. Soubeyroux, H. Touhara, G. Demazeau, F. Langlais, *Mater. Res. Bull.* **16**, 207 (1981).
13. A. Tressaud and G. Demazeau, *High Temp. High Pressures* **16**, 303 (1984).
14. H. K. Mao, P. M. Bell, J. W. Shaner, D. J. Steinberg, *J. Appl. Phys.* **49**, 3276 (1978).
15. J. Rodríguez-Carvajal, paper presented at the 1990 Satellite Meeting on Powder Diffraction (XV Conference of the International Union of Crystallography), Toulouse, 16 to 18 July, 1990, p. 127.
16. K. Suito, N. Kawai, Y. Masuda, *Mater. Res. Bull.* **10**, 677 (1975); S. Endo *et al.*, *High Pressure Res.* **4**, 408 (1990).
17. R. M. Hazen and L. W. Finger, *J. Phys. Chem. Solids* **42**, 143 (1981).
18. J. Haines, J. M. Léger, A. Atouf, in *High Pressure in Material Science and Geoscience. Proceedings of the XXXII Meeting of the European High Pressure Research Group*, Brno, 29 August to 1 September 1994, J. Kamarád, Z. Arnold, A. Kapička, Eds. (Prometheus, Brno, 1994), pp. 133–136.
19. R. W. G. Wyckoff, *Crystal Structures* (Interscience, New York, 1951), vol. I, chap. IV; A. F. Wells, *Structural Inorganic Chemistry* (Oxford Univ. Press, Oxford, ed. 3, 1962), pp. 408, 512, and 520–523.
20. Y. Matsui and M. Matsui, in *Structural and Magnetic Phase Transitions in Minerals, Advances in Physical Geochemistry*, S. Ghose, E. Salje, J. M. D. Coey, Eds. (Springer, New York, 1988), pp. 129–140.
21. N. R. Keskar and J. R. Chelikowski, *Phys. Res. B* **46**, 1 (1992).
22. J. R. Chelikowski, N. Binggeli, N. R. Keskar, *J. Alloys Comp.* **197**, 137 (1993).
23. D. M. Sherman, *J. Geophys. Res.* **98**, 11865 (1993).
24. J. S. Tse, D. D. Klug, D. C. Allan, *Phys. Rev. B* **51**, 16392 (1995).
25. F. Birch, *J. Geophys. Res.* **57**, 227 (1952).

10 October 1995; accepted 7 December 1995

Large-Scale Storms in Saturn's Atmosphere During 1994

A. Sanchez-Lavega, J. Lecacheux, J. M. Gomez, F. Colas, P. Laques, K. Noll, D. Gilmore, I. Miyazaki, D. Parker

Large-scale storms are rarely observed in Saturn's atmosphere, but their appearance traces the wind velocity field, providing information on the vertical structure of the clouds and on the dynamics of the atmosphere. Two large-scale atmospheric disturbances formed by clouds highly reflective in the visible part of the spectrum were observed on Saturn during 1994. An equatorial disturbance with a longitudinal size of ~27,000 kilometers drifted in longitude with a velocity of 273.6 meters per second. A second disturbance, a rapidly evolving convective storm with an initial size ~7000 kilometers, was observed at 56 degrees south, moving with a zonal velocity of 15.5 meters per second.

Cloud systems with enough size and reflectivity contrast to be detected by ground-based telescopes are rare in Saturn's atmosphere (*1–3*). Only five large-scale atmospheric disturbances at different latitudes between 5° and 60°N, known as Great White Spots (GWSs) (*1, 2, 4–9*) and spaced in time by ~30 years, have been observed in the visible part of the electromagnetic spectrum during the last century. The equatorial disturbances (GWS 1876, 1933, and 1990) were characterized by an initial single outburst of bright white clouds (size ≈20,000 km) that showed divergent motions (suggestive of a vigorous upward convection process). After the first 2 weeks of their lives, these GWSs expanded zonally (east-west), with the bright clouds moving away along the parallels, in accordance with the local wind velocity. Once these clouds had encircled the planet (taking about 1 month for the equatorial events), their morphology, occupying a latitude band of about 15°, was formed by a wavy pattern of smaller scale white spots spaced quasi-regularly (size ≈5000 km and lifetime <10 days for these spots). The decay of this activity took place over a few months, during which the patterns lost contrast and the clouds dissipated (*2, 5–7*). The last GWS was observed at the equator in 1990 (*6–9*). After this last disturbance, synoptic-scale short-lived cloud formation occurred in the equatorial region of Saturn during 1991 (*10*), 1992, and 1993.

Here, we report on two disturbances observed at different latitudes during the second half of 1994 (*11, 12*). Most of the images were taken with a CCD (charge-coupled device) camera installed on the dedicated 1-m planetary telescope at Pic-du-

A. Sanchez-Lavega, Departamento de Física Aplicada I, Escuelo Tecnica Superior Ingenieros, Universidad Pais Vasco, Alda. Urquijo s/n, 48013 Bilbao, Spain.
J. Lecacheux, Department des Recherches Spatiales, Observatoire Meudon, 92195 Meudon, France.
J. M. Gomez, Grup Estudis Astronomics, Apartado 9481, 08080 Barcelona, Spain.
F. Colas, Bureau des Longitudes, 77 Avenue Denfert Rochereau, 75014 Paris, France.
P. Laques, Observatoire Pic-du-Midi, 65200 Bagneres de Bigorre, France.
K. Noll and D. Gilmore, Space Telescope Science Institute, 3700 San Martin Drive, Baltimore, MD 21218, USA.
I. Miyazaki, Oriental Astronomical Association, Naha-shi, Okinawa, Japan.
D. Parker, Association of Lunar and Planetary Observers, Coral Gables, FL 33156, USA.